

1 Formation of the hematite-bearing unit in Meridiani Planum: 2 Evidence for deposition in standing water

3 Philip R. Christensen and Steven W. Ruff

4 Department of Geological Sciences, Arizona State University, Tempe, Arizona, USA

5 Received 31 December 2003; revised 30 March 2004; accepted 9 June 2004; published XX Month 2004.

6 [1] The most plausible models for the origin and evolution of a unique geologic unit in
7 Meridiani Planum, Mars, are low-temperature precipitation of Fe oxides/oxyhydroxides
8 from standing water, precipitation from circulating fluids of hydrothermal origin, or the
9 thermal oxidation of magnetite-rich ash. Analysis of Odyssey Thermal Emission Imaging
10 System (THEMIS) infrared and visible images, together with MGS TES, MOLA, and
11 MOC data, has provided additional insight into the Meridiani region. The hematite at
12 Meridiani was most likely derived from a Fe oxyhydroxide precursor such as goethite,
13 is mixed with basalt as the major component, occurs as a thin layer meters to <200 m
14 thick, and is thermophysically distinct from units immediately above and below. Remnants
15 of a hematite-poor unit lie directly above the hematite layer, indicating that hematite
16 formation was sharply confined vertically. The hematite unit appears to embay preexisting
17 channels and occurs only as outliers within closed crater basins, suggesting that it was
18 deposited in a gravity-driven fluid, rather than as a dispersed air fall. The hematite unit lies
19 within a topographic trough over $\sim 3/4$ of its circumference, with the remaining perimeter
20 <150 m lower in elevation. Oxidation of ash during emplacement is unlikely given a
21 goethite precursor and basalt as the major component. Hydrothermal alteration does not
22 account for the confined vertical extent of the hematite layer over large distances and
23 across disconnected outliers. The preferred model is the deposition of precursor Fe
24 oxyhydroxides in water-filled basins, followed by dehydroxylation to hematite in low-
25 temperature diagenesis. This model accounts for (1) the uniform deposition of a thin
26 hematite-bearing unit over an area $\sim 150,000$ km² in size; (2) the transition from hematite-
27 rich to hematite-poor units over less than ~ 10 m vertical distance; (3) the distinct
28 differences from the underlying layers; (4) goethite as the precursor to hematite; (5) the
29 embayment relationships; (6) the occurrence of remnants of the hematite-bearing unit in
30 isolated craters surrounding the main deposit; (7) the lack of other hydrothermal minerals;
31 and (8) the presence of coarse-grained, low-albedo basalt, rather than ash, as the major
32 component. The occurrence of unweathered olivine, pyroxene, and feldspar throughout
33 the equatorial region provides strong evidence that extensive aqueous weathering has not
34 occurred on Mars. Thus the presence of a small number of bodies of standing water
35 appears to represent brief, localized phenomena set against the backdrop of a cold, frozen
36 planet. **INDEX TERMS:** 5410 Planetology: Solid Surface Planets: Composition; 6225 Planetology: Solar
37 System Objects: Mars; 5464 Planetology: Solid Surface Planets: Remote sensing; 3672 Mineralogy and
38 Petrology: Planetary mineralogy and petrology (5410); **KEYWORDS:** hematite, Meridiani, standing water

39 **Citation:** Christensen, P. R., and S. W. Ruff (2004), Formation of the hematite-bearing unit in Meridiani Planum: Evidence for
40 deposition in standing water, *J. Geophys. Res.*, 109, XXXXXX, doi:10.1029/2003JE002233.

42 1. Introduction

43 [2] The Meridiani Planum region, centered near 0°N,
44 0°E, has received special attention following the discovery
45 of gray crystalline hematite from thermal infrared spectra
46 measured by the Mars Global Surveyor (MGS) Thermal
47 Emission Spectrometer (TES) instrument [Christensen *et al.*,
48 *et al.*, 2000b, 2001; Morris *et al.*, 2000; Hynek *et al.*, 2002;

Lane *et al.*, 2002; Arvidson *et al.*, 2003; Lane *et al.*, 2003]. 49
This irregularly shaped unit, centered at $\sim 357^\circ\text{E}$ and 2°S 50
and spanning ~ 500 km in the E-W direction and ~ 300 km 51
N-S, represents the first rock stratigraphic unit mapped on 52
Mars on the basis of the combination of mineralogic and 53
stratigraphic information and was named the Meridiani 54
Formation. The likely role of water in the formation of 55
the hematite deposit [Christensen *et al.*, 2000b, 2001; 56
Hynek *et al.*, 2002; Lane *et al.*, 2002; Arvidson *et al.*, 57
2003; Newsom *et al.*, 2003] led to the selection of this site 58
for in situ exploration by the Mars Exploration Rover 59

60 Opportunity. The Meridiani hematite occurs in a primarily
 61 basaltic unit that is exposed at the top of a sequence of
 62 layered, easily eroded rocks that are stratigraphically above
 63 and postdate the ancient cratered terrain [Presley and
 64 Arvidson, 1988; Edgett and Parker, 1997; Christensen et
 65 al., 2000b, 2001; Hynek et al., 2002; Arvidson et al., 2003].

66 [3] The hematite-bearing unit in Meridiani has a smooth,
 67 flat surface and average rock abundance of $\sim 7\%$ that
 68 provides a safe surface upon which to land and conduct
 69 rover operations. The TES-derived thermal inertia values
 70 range from ~ 170 to 240 (units of $\text{J m}^{-2} \text{s}^{-1/2} \text{K}^{-1}$ used
 71 throughout), corresponding to an average unconsolidated
 72 particle size of $\sim 65\text{--}300 \mu\text{m}$ [Presley and Christensen,
 73 1997]. Within the Rover landing ellipse the albedo ranges
 74 from ~ 0.14 to 0.19 and the dust cover index (DCI) ranges
 75 from ~ 0.96 to 0.98 [Ruff and Christensen, 2002]. These
 76 thermophysical properties indicate that Meridiani is a loca-
 77 tion with little dust accumulation, with a surface that both is
 78 trafficable and will have abundant coarse particles.

79 [4] Several authors have investigated the Meridiani re-
 80 gion using data from the TES, the MGS Mars Orbiter Laser
 81 Altimeter (MOLA), and the MGS Mars Orbiter Camera
 82 (MOC) [Christensen et al., 2000b, 2001; Hynek et al., 2002;
 83 Lane et al., 2002; Arvidson et al., 2003]. The Mars Odyssey
 84 Thermal Emission Imaging System (THEMIS) cameras

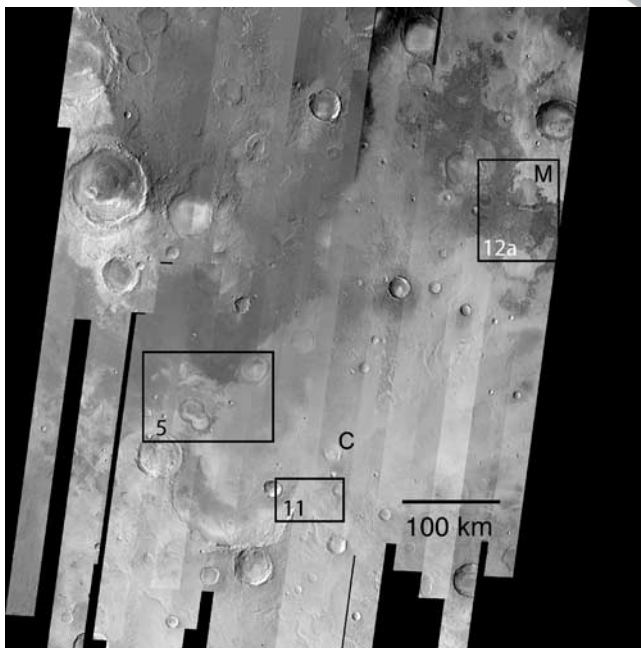


Figure 1. Mosaic of daytime THEMIS infrared images of Meridiani Planum. This mosaic covers the region from 5°S to 5°N and 350° to 360°E . The images were collected at local times from 15.5 to 17.5 H (24 H equal one Martian day). The resolution of each IR image is 100 m per pixel. The locations of features mesa (M) and crater (C) discussed in the text and in Figure 3 are shown for reference, located at the lower left corners of their respective letters. The individual images were normalized prior to mosaicking to reduce temperature differences due to seasonal and local time variations. The outlines of Figures 5, 11, and 12a are shown for reference.

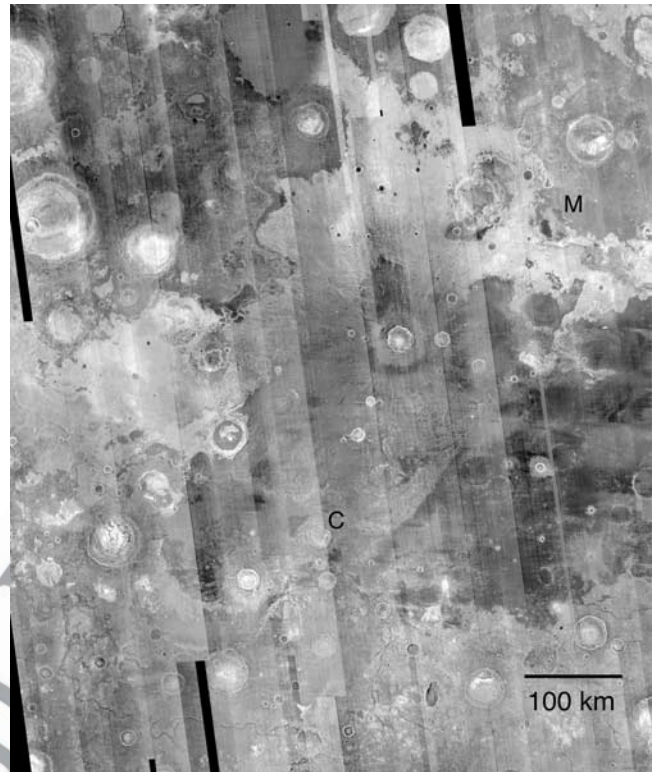


Figure 2. Mosaic of nighttime THEMIS infrared images of Meridiani Planum. This mosaic covers the region from 5°S to 5°N and 350° to 360°E . The images were collected at local times from 3.5 to 5.5 H (24 H equal one Martian day). The resolution of each IR image is 100 m per pixel. The locations of features mesa (M) and crater (C) discussed in the text and in Figure 3 are shown for reference, located at the lower left corners of their respective letters. The individual images were normalized prior to mosaicking to reduce temperature differences due to seasonal and local time variations.

have imaged this region extensively at 100 m per pixel in 85
 day (Figure 1) and night (Figure 2) infrared and 18 m per 86
 pixel in the visible [Christensen et al., 2003a], providing 87
 significantly improved coverage and context imaging for 88
 geologic analysis. In this paper we incorporate these observa- 89
 tions with previous ones to provide additional insights 90
 into the physical properties and regional morphology of the 91
 hematite-bearing unit and its surroundings in order to 92
 further constrain the geologic history of the Meridiani 93
 region. 94

2. Observations and Interpretations 95

2.1. Composition 96

[5] The abundance of hematite in the surface materials of 97
 the hematite-bearing Meridiani Formation (Unit P2 of 98
 Hynek et al. [2002]; Ph of Arvidson et al. [2003]; hereinafter 99
 referred to as Ph) has been determined using linear decon- 100
 volution of TES spectra [Ramsey and Christensen, 1998; 101
 Bandfield, 2002] to vary from $\sim 5\%$ to $\sim 20\%$. The derived 102
 hematite abundance depends on the particle size of the 103
 hematite end-member used in the deconvolution model 104

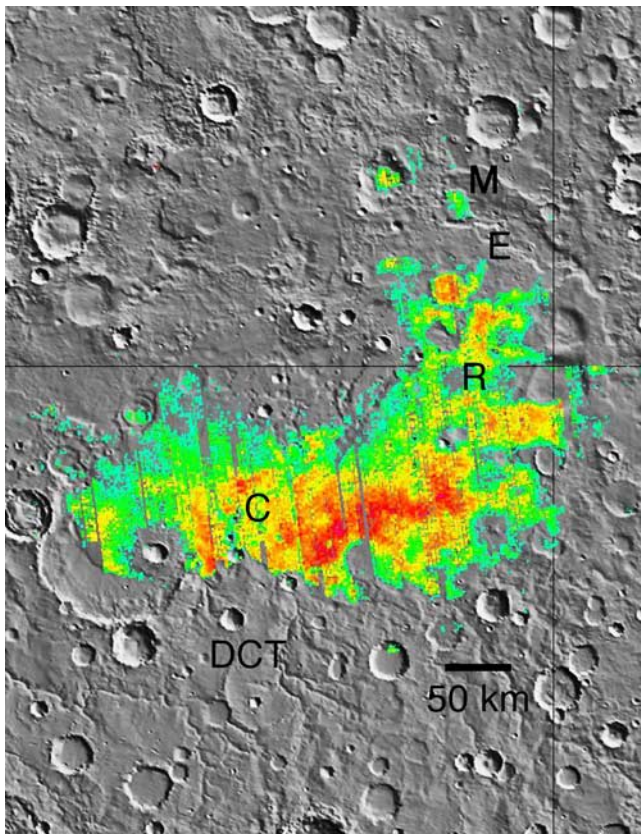


Figure 3. Occurrence of hematite-bearing units in Meridiani Planum. The hematite abundance derived from TES data is shown superimposed on a shaded relief image derived from MOLA data [Smith *et al.*, 2001]. The TES hematite abundances vary from $\sim 5\%$ (blue) to $\sim 20\%$ (red). Data where the hematite spectral signature was less than a detectable limit of $\sim 5\%$ have been set to zero (transparent). The positions of specific areas rise (R), mesa (M), and crater (C) discussed in the text are located at the lower left corners of their respective letters. The location of representative occurrences of Etched (E) and dissected cratered terrain (DCT) of Arvidson *et al.* [2003] are indicated by letters. A conservative lower hematite detection limit was applied to this figure to emphasize locations with strong hematite signatures. Vertical and horizontal lines are at 0° longitude and 0° latitude, respectively.

105 because of the variation in spectral band depth with particle
 106 size. However, an upper limit of hematite abundance can be
 107 determined using the depth of the silicate spectral feature
 108 from 8 to $14 \mu\text{m}$. The emissivity of this feature is 0.955
 109 [Christensen *et al.*, 2001] compared to a value of 0.945
 110 observed in TES spectra for regions mapped as 100% basalt
 111 [Christensen *et al.*, 2000a]. Thus the silicate band is reduced
 112 by only 20%, providing the upper limit on hematite where it
 113 is most abundant. Figure 3 shows a map of hematite
 114 abundance derived from TES spectra, scaled to give a
 115 maximum abundance value of 20%.

116 [6] Laboratory thermal emission measurements of hema-
 117 tite samples show variations in spectral properties for
 118 samples derived from different precursor minerals and by
 119 different processes [Glotch *et al.*, 2004]. Hematites derived

from high-temperature oxidation of synthetic magnetites 120
 provide a poor fit to the TES spectra from Meridiani, while 121
 hematites derived by lower-temperature ($\sim 300^\circ\text{C}$) dehy- 122
 droxylation of synthetic goethite are an excellent match to 123
 the TES spectra [Glotch *et al.*, 2004]. Natural hematite 124
 samples that provide good spectral matches to the TES 125
 spectra also appear to have been derived from goethite 126
 precursors on the basis of XRD and Mössbauer character- 127
 ization [Glotch *et al.*, 2004]. The lowest temperature at 128
 which goethite converted to hematite under dry laboratory 129
 conditions in the experiments of Glotch *et al.* was 300°C . 130
 However, it has been shown experimentally that under wet 131
 conditions, goethite will convert to hematite within weeks at 132
 100°C [Tunell and Posnjak, 1931], and Berner [1969] 133
 calculated that the maximum temperature at which goethite 134
 is thermodynamically stable relative to hematite plus water 135
 is $\sim 40^\circ\text{C}$. 136

[7] An atmospherically corrected surface spectrum of the 137
 hematite-bearing surface is shown in Figure 4. This spec- 138
 trum closely resembles the spectrum of typical Syrtis Major 139
 basalt [Christensen *et al.*, 2000a; Bandfield *et al.*, 2000] 140
 once the hematite spectral contribution has been subtracted 141
 (Figure 4). The basalt-like shape of TES spectra from 142
 Meridiani, along with the relatively low albedo (0.14– 143
 0.18) and dust index [Ruff and Christensen, 2002], provides 144
 strong evidence that coarse-grained ($\geq \sim 100 \mu\text{m}$), dust-free 145
 basalt is the major component in this region. No minerals 146
 other than hematite and the plagioclase, pyroxene, and 147
 olivine found in typical Martian basalts [Christensen *et al.* 148
et al., 2000b; Bandfield, 2002] have been identified in Ph. 149

[8] The abundance of hematite currently exposed at the 150
 surface does not show any systematic variation across 151
 the deposit (Figure 3). Similar, high abundances occur in 152
 the eastern, central, and far northern portions of the unit, 153
 and moderate abundances occur near the southwestern 154

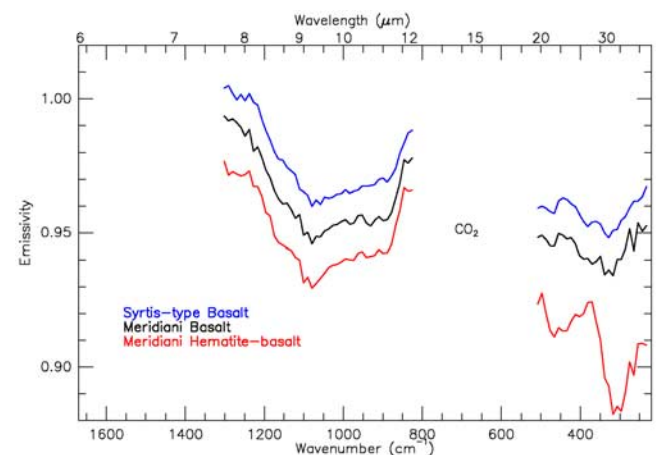


Figure 4. Comparison of atmospherically corrected TES spectra of Meridiani Planum and Syrtis-type (Type I) basalt. The red spectrum is an average of 30 TES spectra from orbit 5499 following deconvolution using the 7 TES surface and atmosphere end-members [Bandfield *et al.*, 2000]. The hematite component has been subtracted from the red spectrum to produce the black spectrum, revealing that the nonhematite component of Meridiani Planum is remarkably similar to Syrtis-type basalt.

margin. There is no strong correlation with elevation derived from the Mars Global Surveyor MOLA experiment [e.g., *Smith et al.*, 2001]. Regions of high hematite abundance at -2.5°S between 354.2° and 358.7°E (Figure 3) vary in elevation from -1550 to -1300 m, and local variations of ~ 100 m over 25 km distance show no significant variation in hematite abundance.

[9] In summary, the hematite at Meridiani varies in abundance from 0 to 20%, was most likely derived from a Fe oxyhydroxide precursor such as goethite, shows no coherent spatial variation in abundance or spectral character, and is mixed with a low-albedo, plagioclase/pyroxene/olivine basalt as the major component.

2.2. Thermophysical Properties

[10] The THEMIS daytime temperature images of the Meridiani region (Figure 1) show large variations that are due to solar illumination effects on topography and the thermophysical properties of thermal inertia and albedo [Christensen *et al.*, 2003a]. Local temperature variations associated with variations in thermal inertia are among the largest observed on the planet [Christensen *et al.*, 2003a]. The THEMIS nighttime temperatures (Figure 2) also show significant differences that correlate with the daytime patterns and are due to thermal inertia variations.

[11] A comparison of the distribution of hematite abundance (Figure 3) and the THEMIS mosaic reveals a close correlation between the hematite-bearing unit and surfaces that appear uniform and relatively warm (bright) in the daytime mosaic. This correlation is especially apparent along the northwest margin of Ph, where the hematite-bearing unit occurs in isolated patches associated with filled craters and intercrater mesas (Figure 5).

[12] The hematite abundance along the margins of the hematite-bearing unit drops from detectable to nondetectable levels across neighboring TES pixels spaced 3 km apart (Figure 3) [Christensen *et al.*, 2001]. This abrupt change in hematite abundance correlates with the change in morphology between the layered unit Ph and the dissected ancient cratered terrain to the south (unit DCT of *Arvidson et al.* [2003]) and the etched surface to the north (unit E of *Arvidson et al.* [2003]) (Figure 3). No hematite is detected away from Ph.

[13] Surfaces of Ph that contain hematite have been determined from THEMIS nighttime IR images to be $\sim 6\text{--}8$ K colder (~ 192 K versus ~ 198 K) at night than units that are stratigraphically lower (Figure 2). These data were taken at 3.1 H (24 H equals one Martian day), aerocentric longitude (L_s) of $\sim 345^{\circ}$. These temperature differences correspond to differences in thermal inertia of $80\text{--}100$ [Ferguson and Christensen, 2003]. The thermal inertia of Ph derived from TES data [Mellon *et al.*, 2000; *Arvidson et al.*, 2003] ranges from ~ 170 to 240, corresponding to a grain size of $\sim 65\text{--}300$ μm , assuming well-sorted, unconsolidated spheres [Presley and Christensen, 1997].

[14] The sharp compositional boundary and particulate nature of the uppermost surface of Ph indicate that the hematite-bearing unit is covered with loose material that has been derived from an underlying, in-place rock unit [Christensen *et al.*, 2001]. As this rock unit disaggregates, the hematite-bearing component either is too coarse to be

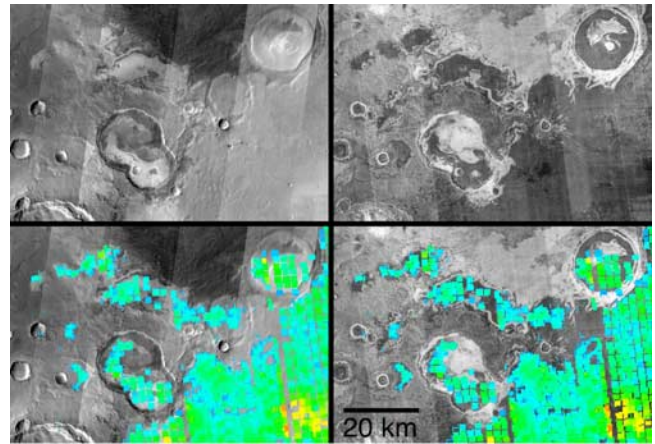


Figure 5. Hematite occurrence in series of outliers to the northwest of the main Ph unit. The hematite abundances were derived from TES and vary from $\sim 5\%$ (blue) to 20% (red). The TES data are superimposed on mosaics of day (left column) and night (right column) THEMIS infrared images. The hematite-bearing materials have similar thermal properties. Seen at THEMIS resolution, these materials occur only in the uppermost layer of the stack of layered materials that form these outliers of Ph. The two major outliers in this region occur within a double crater and on a circular mesa interpreted to be the remnant floor of a crater whose walls have been completely removed. The lower hematite abundance threshold is slightly lower than in Figure 3 to emphasize the strong correlation between morphology and hematite occurrence.

transported by the wind or becomes fine grained enough to be widely dispersed in suspension.

[15] Preliminary mapping of this area has not revealed any overall correlation of hematite abundance with the thermal inertia properties of Ph. However, locally, the contacts between thermal units correlate with variations in hematite abundance (Figures 2 and 3), possibly indicating subtle differences between different stratigraphic layers.

[16] Unit Ph has a lower thermal inertia than the etched unit E on which it was deposited [Hynek *et al.*, 2002; *Arvidson et al.*, 2003]. The partially exhumed craters and intercrater mesas on the western margin of Ph (Figure 5) provide additional insights into the nature of Ph itself. Eroded portions of Ph in this region show that the materials within Ph that underlie the exposed hematite unit have higher thermal inertia (relatively warm at night and cold in the day) than the uppermost layer of Ph (Figure 5). This observation indicates that the uppermost portion of Ph is either less indurated or erodes to less consolidated material than the materials below. This lower component of Ph is layered at THEMIS visible image scale and has a significantly different morphology than the etched unit E. We interpret these relatively high-inertia layers to be a subunit in Ph that lies below the hematite-bearing unit. These observations suggest that the hematite layer itself is a thin unit at the top of Ph.

[17] A relatively bright layer can be seen immediately below the uppermost dark unit, where it is exposed in the walls of impact craters. This bright unit is seen in craters as

245 small as ~ 500 m in diameter in the vicinity of the MER-B
 246 landing ellipse (Figure 6). These craters are only ~ 20 deep,
 247 indicating that the bright layer is < 20 m below the surface.
 248 A similar bright unit is found several tens of meters below
 249 the surface in the northeastern portion of Ph, where it is
 250 exposed along the steeply eroded margin of Ph and in the
 251 walls of two impact craters (Figure 7). The thickness of the
 252 Ph unit above the Etched unit is several hundred meters (see

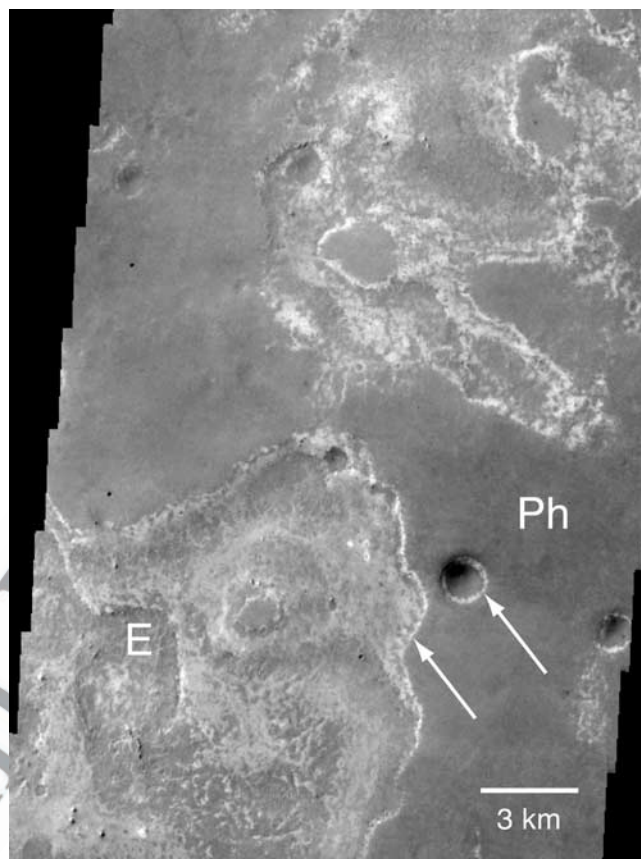


Figure 7. The regional context of a relatively bright layer immediately below the hematite-bearing upper layer of Ph as seen at 36-m resolution by the THEMIS visible camera. This unit is suggested to be the same unit as seen ~ 300 km to the southwest within the MER-B landing ellipse (Figure 6). This layer is exposed within an inner crater wall and at the margin of the Ph unit (arrows). The etched unit (E) occurs in the lower left corner of this image, several hundred meters below the bright unit. Occurrences of this bright layer occur throughout Ph; this example is in the northeast region of Ph, near rise R. This portion of THEMIS visible image (V03570003) is centered at 0.45°N , 358.6°E .

below), so this bright unit appears to lie within Ph. Exposure of this subunit, rather than unit E as suggested by Arvidson *et al.* [2003], may produce the variation in albedo and thermal properties seen within the MER landing ellipse.

Figure 6. High-resolution MOC image (E01203255) (M. C. Malin *et al.*, E12-03255, Malin Space Science Systems Mars Orbiter Camera Image Gallery, http://www.msss.com/moc_gallery/, 2002) of the relatively bright layer immediately below the hematite-bearing upper layer of Ph within the MER-B landing ellipse. This unusual unit appears to lie less than several tens of meters below the surface throughout this region. It is seen exposed in the walls of craters < 500 m in diameter that are $< \sim 20$ m deep and is interpreted to be a subunit within Ph. Image is ~ 3 km wide and ~ 10 km long, centered near 354.1°E , -1.9°S with a resolution of 3 m per pixel.

257 We suggest that this distinctive unit extends over large
 258 portions of the Ph unit, possibly being a single “marker”
 259 bed that occurs beneath the overlying hematite unit through-
 260 out Ph and formed under similar conditions over a relatively
 261 short period of time.

262 [18] Three subunits of Ph can be identified laterally on the
 263 basis of minor differences in their relative thermal inertias
 264 derived from the nighttime THEMIS images (Figure 2).
 265 Ph-a is a relatively cold (~ 185 K at a local time of 3.1 H,
 266 $L_s \sim 340^\circ$) unit with a relatively low thermal inertia of
 267 ~ 150 , corresponding to an average particle size for uniform,
 268 unconsolidated grains of ~ 40 μm [Presley and Christensen,
 269 1997]. This subunit covers over half of Ph, including the
 270 western portion of the MER landing ellipse. Ph-b is an
 271 intermediate inertia unit with relatively uniform nighttime
 272 temperatures of 189–190 K (3.1 H, $336^\circ L_s$), corresponding
 273 to an average particle size of ~ 125 μm , that covers $\sim 30\%$ of
 274 Ph. This unit occurs in the eastern portion of the landing
 275 ellipse. Finally, subunit Ph-c is thermally heterogeneous at
 276 spatial scales of ~ 0.3 to 1 km with temperature variations of
 277 187–195 K covering $\sim 20\%$ of Ph but not exposed within
 278 the landing ellipse. These temperatures correspond to thermal
 279 inertias of ~ 200 – 300 , respectively, which correspond to
 280 average particle sizes of ~ 125 – 750 μm .

281 [19] In summary, hematite-rich material occurs as a dis-
 282 aggregated surface veneer of an in-place geologic unit.

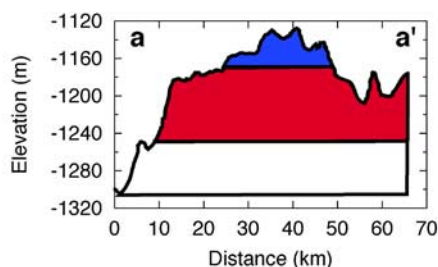
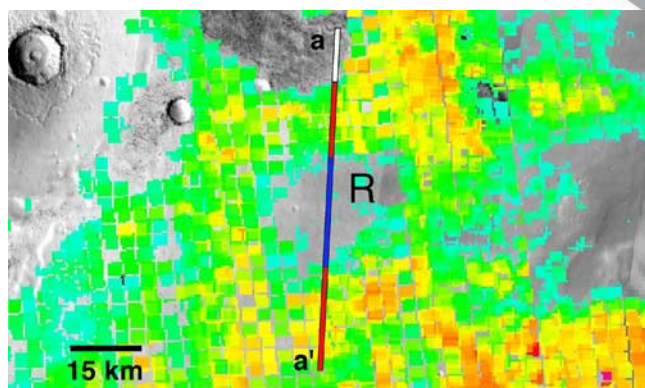


Figure 8a. The hematite-free unit (Pu) at rise R. The hematite abundance derived from TES data is superimposed on a mosaic of THEMIS daytime IR images. The hematite detection threshold is the same as in Figure 3. A topographic profile (a-a') derived from MOLA gridded data shows that the hematite-free unit (Pu), indicated by the blue bar on the image and the blue layer in the topographic profile, is stratigraphically above unit Ph. The distribution of the hematite-free unit is indicated by the red bar and red layer; the location of the hematite-free unit below Ph is indicated by the white bar and white layer.

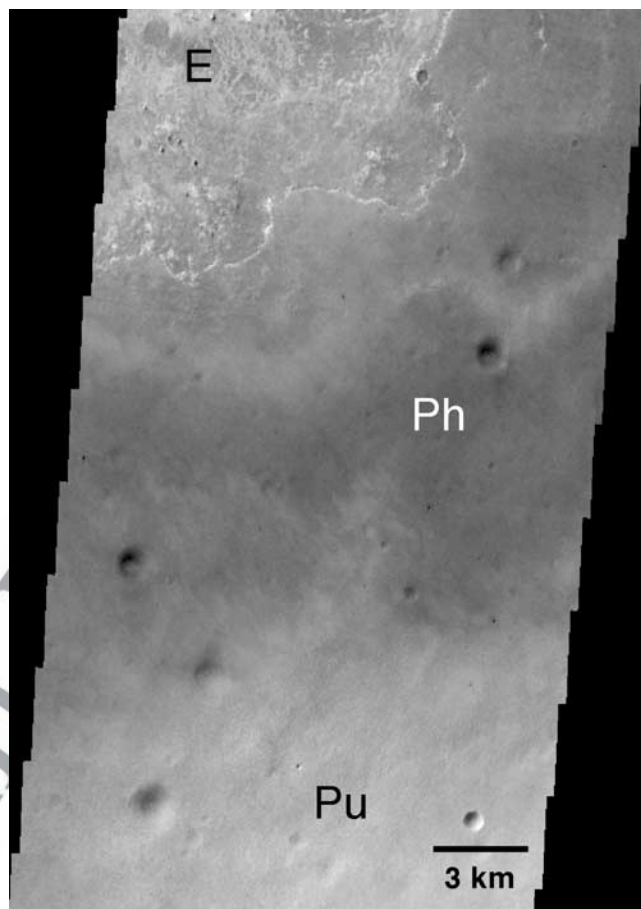


Figure 8b. The contact between the hematite-bearing unit Ph and the overlying hematite-free unit Pu at rise R. The hematite-free etched (E) unit can also be seen in the upper left portion of the image at location “a” in Figure 8a, where the overlying Ph unit has been removed by erosion. THEMIS VIS image V03570003 centered at 0.17°N , 358.5°E . Image resolution is 36 m per pixel.

Hematite is not transported in detectable abundance beyond 283 the margin of this unit. The uppermost surface of Ph has a 284 lower thermal inertia than the underlying etched unit E, and 285 subunits with higher inertia occur within Ph. A thin, 286 relatively bright layer in the vicinity of the MER-B ellipse 287 is proposed to be a layer within Ph that lies just below the 288 hematite-bearing material. A layer of similar thickness and 289 appearance is exposed in Ph ~ 300 km away, suggesting that 290 this unit may be common beneath the hematite unit and that 291 it and the hematite unit may be genetically related. 292

2.3. Stratigraphic Relationships 293

[20] A key question to the origin of hematite is its 294 distribution within and above unit Ph. Insights into this 295 question are found in two regions within the boundaries of 296 the main Ph unit that have little or no hematite exposed on 297 the surface. The first is a 25-km-wide rise centered near 298 358.4°E , -0.2°S (R in Figure 3). The surface of this rise 299 is up to 50 m above the hematite-rich plains (Figure 8a). There 300 is a distinct topographic break in slope associated with the 301 margins of this rise. At the locations of the breaks in slope 302 that define the margins of this rise, there is a sharp decrease 303

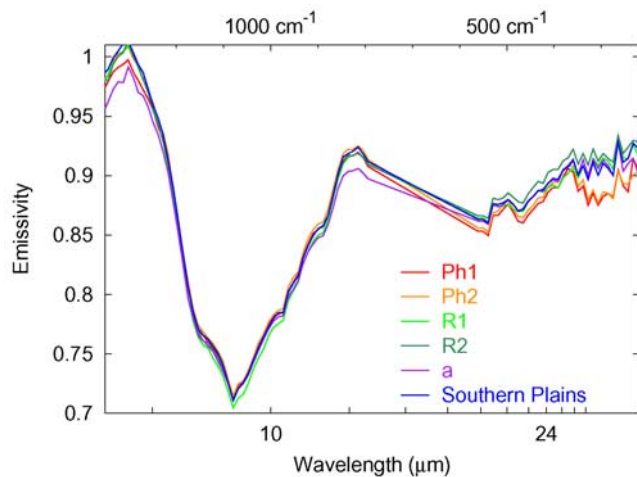


Figure 9a. TES spectra of the hematite-poor surface of rise R compared to the hematite-rich Ph unit. Spectra over the spectral range from 1350 to 350 cm^{-1} are shown from a region of high hematite immediately south of R (Ph1) and a second region ~ 50 km farther south (Ph2). Spectra from rise R (R1 and R2) are from two consecutive TES observations. Spectra from surfaces that do not have hematite (a and Southern Plains) are shown for reference. The surface of rise R has significantly less hematite than the neighboring Ph surfaces, and the abundance on this surface is comparable to hematite-free plains. All spectra are from a single TES orbit and are averages of all six detectors collected simultaneously, covering an area ~ 9 by 6 km in size.

in hematite abundance (Figure 8a). Figures 9a and 9b shows TES spectra acquired on a single orbit that crosses the boundary between the hematite-rich Ph surface and the rise R. As seen in Figures 9a and 9b, the two hematite absorptions at ~ 300 and 480 cm^{-1} are readily apparent in the representative spectra from unit Ph at band depths corresponding to abundances of $\sim 15\%$. The depths of these absorption bands are significantly reduced or absent in the spectra from the rise. This marked decrease in hematite band depth in the material on rise R indicates that this overlying material has significantly less hematite than the material immediately below.

[21] The topography and hematite abundance observations suggest that the material that comprises rise R is a stratigraphic unit (designated Pupper or Pu) that lies immediately above the hematite-bearing unit of Ph. The transition from hematite-rich to hematite-poor materials occurs over a maximum vertical distance of ~ 20 m (Figure 8a) and may occur at the contact between Ph and Pu.

[22] A THEMIS visible image of this area (Figure 8b) shows that the morphology and crater abundance of Ph and Pu are similar. The contact is gradational, with isolated remnants of the overlying Pu unit occurring away from the main body, indicating that this unit was removed by erosion. The overlying Pu unit appears to lie conformably on the hematite-bearing unit, with no evidence that Ph underwent erosion prior to the deposition of the overlying unit. This relationship suggests that there was no significant gap in time between the deposition of the two units. The gradational character of the contact also indicates that there are no

significant differences in the competency of the two units, suggesting that the two units were deposited under similar conditions and processes.

[23] A similar example of an overlying, hematite-poor layer is observed in an eroded, 30-km-wide mesa (Figure 10) centered at 358.5°E , 2.5°N near the northern margin of Ph (M in Figure 3). This unit appears to lie directly on top of the dissected cratered terrain unit at this location, without the intervening etched unit. As discussed by *Arvidson et al.* [2003], the etched unit lies unconformably on top of unit DCT throughout Meridiani. It appears that in some locations, such as a mesa M, unit Ph also lies unconformably on top of the DCT.

[24] Hematite abundance varies across mesa M, decreasing significantly on the eastern and western margins (Figure 3). These hematite-poor surfaces rise ~ 20 – 30 m above Ph. The Ph surface exposed in the center of the mesa is smoother than the hematite-poor surfaces, which have a distinctive erosional texture of subtle pits at 100-m scales and resemble subtle surface textures at rise R. As seen at R, the overlying surface at M appears to lie conformably on top of the hematite unit, with no evidence for a significant change in depositional environment and no evidence for a discontinuity in time between the deposition of the two units.

[25] The low abundance of hematite on the overlying layer provides strong evidence that hematite is not a lag deposit eroded from the overlying layers because it should be present in significant amounts on the surface of these overlying layers as well if it was contained within them. Therefore it appears that the hematite originates from the layer where it is currently observed.

[26] The eastern slope of the mesa at M is 3–5 km wide and exposes the entire Ph unit down to the dissected cratered terrain on which it appears to lie (Figure 10). This slope is wide enough to be resolved by TES yet has no detectable hematite. The lack of hematite on this slope suggests that the lower layers of Ph may not contain hematite. The southwest margin of Ph near 352.8°E , 3.2°S

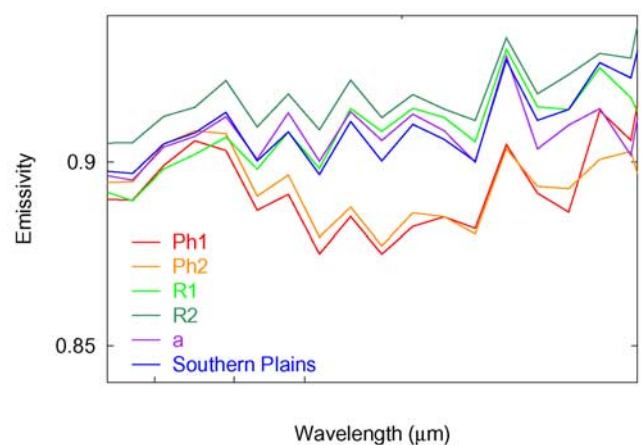


Figure 9b. TES spectra of the hematite-poor surface of rise R compared to the hematite-rich Ph unit over the spectral range 400 to 220 cm^{-1} . This spectral region contains the strong hematite absorption band observed by TES.

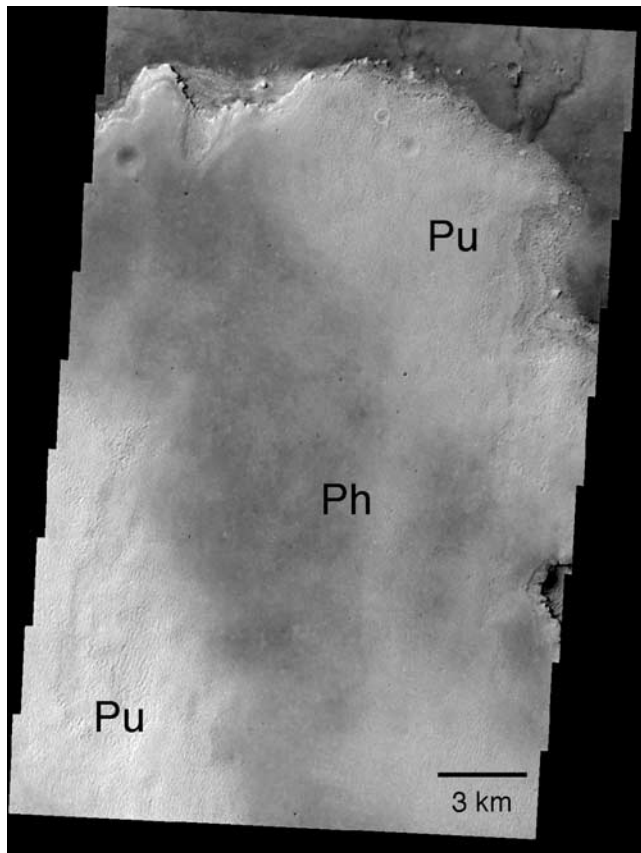


Figure 10. The surface of mesa M. Outcrops of the hematite-free unit (Pu) occur on the western and eastern margins of this mesa. The central portion is topographically lower than the margins and has hematite exposed on the surface. The older dissected cratered terrain on which the Ph and Pu units were unconformably deposited can be seen in the upper right portion of this image. THEMIS visible image V03280003, centered at 2.7°N, 358.4°E. Image resolution is 18 m per pixel.

372 is also a broad gentle slope on which the entire thickness of
373 Ph again is exposed. The TES hematite abundance
374 decreases down this slope, suggesting that hematite may
375 occur only in the topmost layer.

376 [27] The nighttime temperatures of M on the eastern and
377 western hematite-free surfaces are 6–12 K colder than the
378 central hematite-rich surface (Figure 2). These temperature
379 differences indicate that the hematite-rich surface, while
380 typically lower thermal inertia than the surrounding etched
381 and dissected cratered terrains, has a higher inertia than the
382 material stratigraphically above. This observation is consistent
383 with the nearly complete removal of a slightly less
384 competent overlying layer down to current surface of Ph.

385 [28] The southern margin of the hematite unit appears to
386 embay the highstanding terrain to the south (Figure 11), as
387 originally noted by *Edgett and Parker* [1997] and discussed
388 by subsequent authors [*Christensen et al.*, 2000b; *Hynek et al.*,
389 2002]. This relationship suggests that the hematite-bearing
390 unit was originally deposited in a dense, gravity-
391 controlled fluid, rather than as a dispersed, air fall layer.

392 [29] There are only three occurrences of the hematite-
393 bearing unit exposed south of the main Ph deposit (Figure 3).

All occur within craters that are 20–40 km in diameter and
are within 50 km of the southern margin. All of these
occurrences appear to be eroded remnants of once-larger
deposits. The elevations of the upper surfaces of these
outliers are ~300–700 m below the average level of the
top of the main hematite-bearing unit and ~200–700 m
below their respective crater rims. No hematite is observed
on the intracrater plains of the ancient cratered terrain south
of Ph, which vary in elevation from several hundred meters
below to several hundred meters above the hematite-bearing
unit. This lack of any detectable hematite on the plains units
indicates that either hematite material was not deposited as a
widely distributed air fall or this material has been completely
removed from the plains surfaces.

[30] Finally, the morphologic and thermophysical properties
of the Etched and Ph units are different, as reflected in the
fact that these materials have been mapped as distinct units
on the basis of these properties [*Hynek et al.*, 2002; *Arvidson et al.*,
2003]. Figure 12 shows two THEMIS VIS images and a mosaic of
THEMIS IR images that illustrate the significant differences in the
properties of these units. Possible causes are (1) differences in
density and porosity between igneous and clastic sedimentary
materials or among igneous materials; (2) variations in particle
size and sorting among different sedimentary deposits; and (3)
variations in the degree of lithification or cementation among
initially similar clastic or pyroclastic materials [*Christensen et al.*,
2003a]. Whatever the cause, the observed differences in
morphologic and thermophysical characteristics between the Etched
and Ph units imply temporal changes in the processes or environments
that formed them.

[31] In summary, the hematite-bearing unit appears to be a
relatively thin upper unit in Ph, with higher-inertia material
immediately below. The occurrence of hematite-free units directly
above the hematite unit provides strong evidence that whatever
mechanism formed the hematite was sharply confined vertically
and/or in time. The hematite unit appears to embay preexisting
channels, occurs as outliers within closed crater basins, has
significantly different properties from the Etched unit below it,
and is absent from the

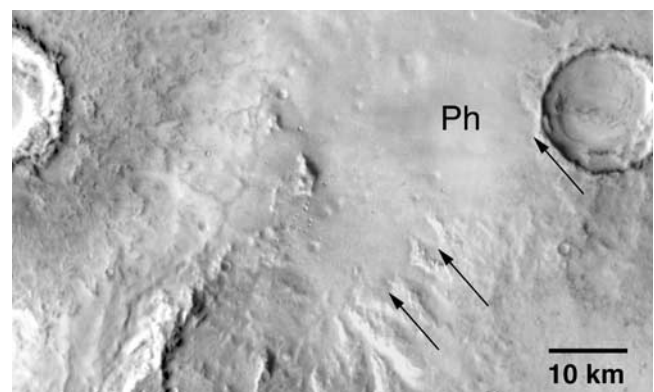


Figure 11. Embayment relationships on the southern margin of the hematite-bearing unit Ph. The location of the embayment margin is indicated by arrows. This daytime infrared image is an enlarged and image-enhanced segment of Figure 1. Image resolution is 100 m per pixel.

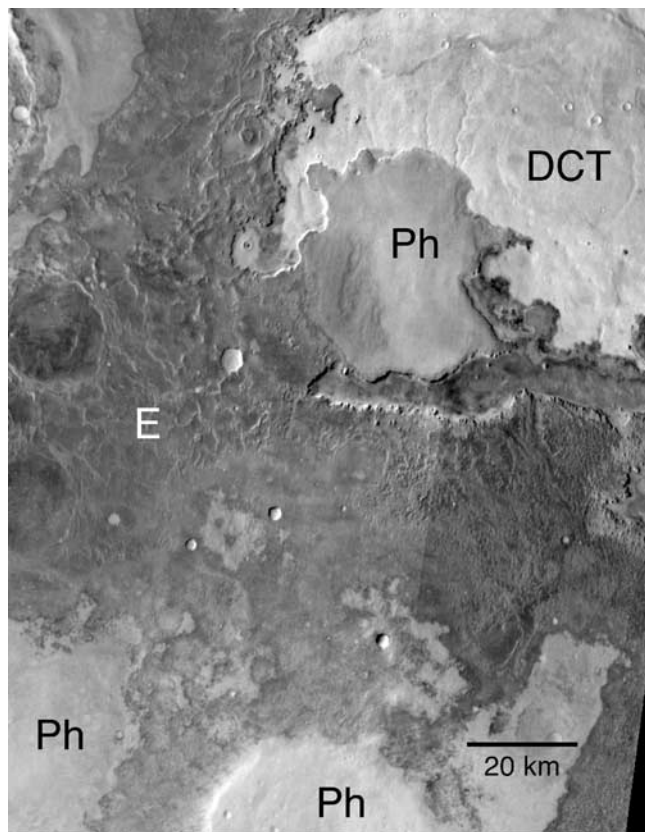


Figure 12a. Comparison of surface morphology of the hematite-bearing unit (Ph), the lower etched unit (E), and the dissected cratered terrain (DCT). The Ph unit in the upper right portion of the figure is the mesa (M) in Figures 1, 2, 3, and 10. It is characterized by a smooth surface with layers exposed in eroded slopes. The etched unit appears to be eroded into a series of ridges and small mesas. The Ph unit appears to have been deposited unconformably on the etched unit. The cratered terrain is the oldest surface, and both the Ph and E units were deposited unconformably on this unit. A series of channels were eroded into the DCT unit prior to the deposition of Ph. These channels slope southward toward the current location of the Ph unit in mesa M. The semicircular occurrence of Ph in the lower center of the figure is a portion of a circular deposit interpreted to have been formed within the walls of a crater basin that has since been completely removed. This figure is an enlarged portion of the daytime infrared mosaic shown in Figure 1. Image resolution is 100 m per pixel.

435 surrounding plains, suggesting that it may have been
436 deposited in a dense fluid, rather than as a dispersed air fall.

437 2.4. Topographic Relationships

438 [32] A series of eight topographic profiles taken across Ph
439 are shown in Figures 13a and 13b. Along the length of the
440 southern margin of Ph the contact is a local topographic
441 minimum, with the cratered highlands rising several hundred
442 meters to the south and the hematite unit rising 100–400 m to
443 the north, typically with a convex upward slope (Figures 13a
444 and 13b). The elevation of the hematite unit above the contact
445 increases from a low of ~100 m in the east to ~150–200 m in
446 the central region to a maximum of ~400 m in the southwest.

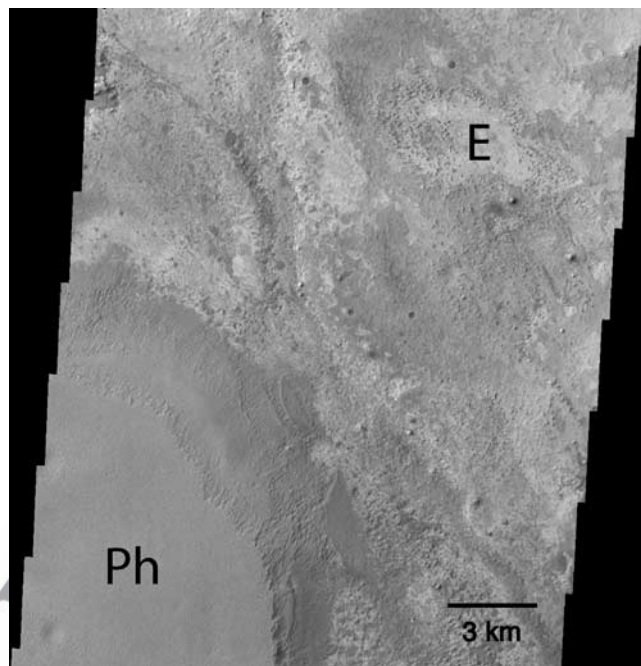


Figure 12b. Comparison of the textures of the etched unit E and the hematite-bearing Ph unit. This THEMIS visible image shows the contact of Ph with the underlying etched unit E. This portion of THEMIS image V03520003 covers an area 18 km × 20 km in size, centered near 1.2°N, 0.5°E with a resolution of 18 m per pixel.

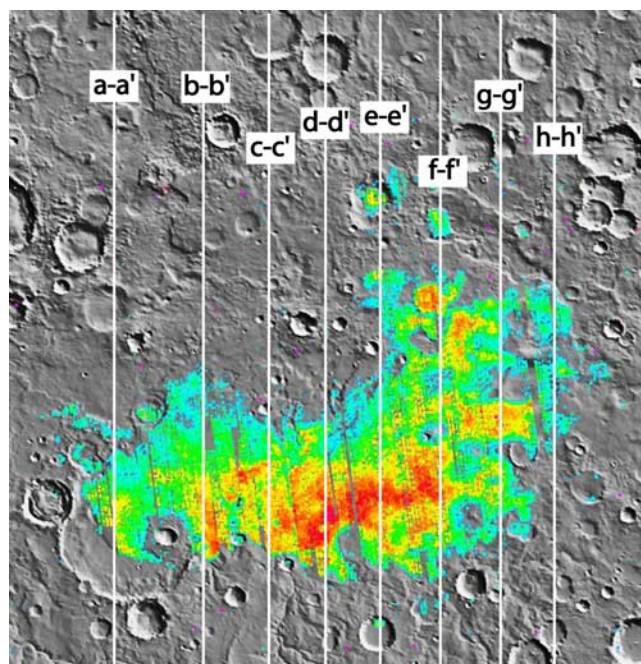


Figure 13a. The location of topographic profiles across Meridiani Planum. The positions of eight profiles are shown on a map of hematite abundance derived from TES data and a MOLA-derived shaded relief image. Hematite abundances vary from ~5% (blue) to ~20% (red).

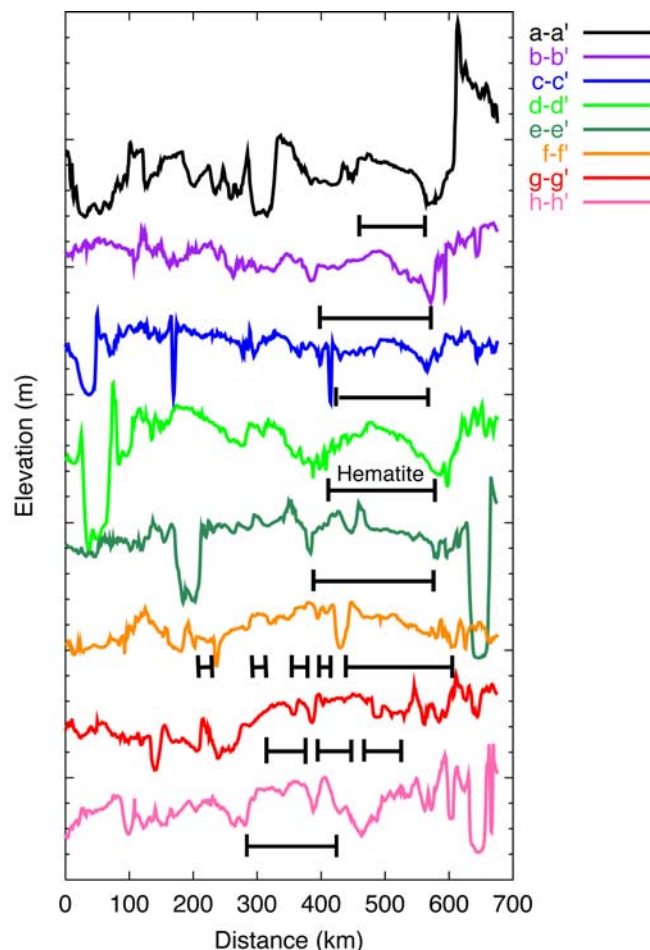


Figure 13b. Topographic profiles for the locations shown in Figure 13a. The location of the hematite-bearing unit (Ph) of the Meridiani Formation is shown by horizontal bars on each profile. The vertical elevation scale is 200 m per tic; profiles have been vertically offset for clarity. Unit Ph is in a topographic trough in profiles a-a' through e-e' and is bounded by a topographic rise to the south on all profiles except f-f'. Unit Ph is 50–150 m higher than the bounding units to the north in the three eastern profiles, f-f', g-g', and h-h'.

447 This increase in apparent unit thickness toward the west may
 448 be due to deposition within a preexisting 140-km-diameter
 449 crater (Figures 13a and 13b). Along the western margin,
 450 Ph rises ~250 m from the nearby plains.

451 [33] Along its northern and eastern boundary, Ph is in
 452 contact with several different units that are interpreted to
 453 predate Ph [Christensen *et al.*, 2001; Hynek *et al.*, 2002;
 454 Arvidson *et al.*, 2003; Newsom *et al.*, 2003]. There is typically
 455 less than 50 m of elevation change across this contact, and
 456 in the central and western sections the bounding units are
 457 50–100 m higher than Ph (Figures 13a and 13b; profiles a-a'
 458 through f-f'). North of the contact the bounding Ph and E units
 459 typically vary in elevation by only ± 50 m over a distance up to
 460 250 km from the hematite unit (Figures 13a and 9b).

461 [34] The northern, eastern, and western margins of Ph are
 462 discontinuous with numerous outliers up to 60 km in size and
 463 separated by up to 200 km from the main deposit (Figure 3).

In many cases these outliers have exposed layers and margins 464
 interpreted to have receded by erosion [Arvidson *et al.*, 2003; 465
 Newsom *et al.*, 2003]. Along the central portion of the 466
 northern boundary, these outliers may be eroded remnants 467
 of a once continuous layer [Christensen *et al.*, 2000b, 2001; 468
 Hynek *et al.*, 2002; Arvidson *et al.*, 2003; Newsom *et al.*, 469
 2003]. However, the most distant outliers occur within large 470
 (>30- to 45-km-diameter) craters or as circular or quasi- 471
 circular deposits surrounded by circular troughs, suggesting 472
 that they were also deposited inside preexisting craters whose 473
 rims have since been removed by erosion. The lack of 474
 hematite material exposed on the plains between the main 475
 Ph unit and the occurrence of these distant outliers may 476
 indicate that these outliers were deposited within isolated 477
 closed crater basins and that the hematite-bearing unit was 478
 not deposited as a continuous layer over the entire surface. 479

[35] Nine craters ranging in diameter from 2 to 25 km 480
 within Ph have either excavated through or deposited ejecta 481
 on Ph, resulting in low hematite abundance at TES resolu- 482
 tion (Figure 3). These craters are centered, from east to 483
 west, at 353.8°E, -3.0°S (22-km diameter), 354.8°E, 484
 -2.7°S (10-km diameter), 355.6°E, -2.7°S (7-km diame- 485
 ter), 356.4°E, -2.8°S (6-km diameter), 356.9°E, -3.3°S (2- 486
 km diameter), 357.6°E, -2.5°S (5-km diameter), 357.8°E; 487
 -1.2°S (7-km diameter), 358.3°E, -1.2°S (11-km diameter), 488
 and 358.3°E, -2.3°S (9-km diameter). Thermally distinct 489
 crater ejecta rays from many of these craters are present on 490
 Ph (Figure 2), indicating that they postdate the unit's 491
 formation. The lack of detectable hematite on the ejecta 492
 from these craters, including one only ~2 km in diameter, 493
 suggests that the hematite-bearing layer is significantly 494
 thinner than the depth to which these craters excavated 495
 ($< \sim 0.2$ km [Melosh, 1989]). 496

[36] A 22-km-diameter impact crater located at 354.9°E, 497
 -2.3°S has hematite-bearing material draping the NW wall 498
 and onto the floor (Figure 3; C). The upper surface of the 499
 hematite unit drops ~180 m in 3.5 km (3° slope) down the 500
 NW inner crater wall and then an additional 200 m over 501
 11 km (1° slope) across the crater floor. In the SE region 502
 of the crater the floor materials drop an additional 120 m in 503
 3.5 km (2° slope). Truncated rock layers are exposed along 504
 this slope, indicating that this is an erosional surface. This 505
 lowest region of the crater does not have hematite exposed 506
 at the surface (Figure 3), suggesting that the hematite- 507
 bearing unit has been completely removed by erosion in 508
 this area. Unit Ph clearly drapes the preexisting topography 509
 at this location and was deposited either subaerially or 510
 subaqueously onto an older landscape. No distinctive mor- 511
 phologies are observed to distinguish these two modes, and 512
 the slopes of these surfaces are low enough (1°–3°) to 513
 permit either process to have occurred. 514

2.5. Morphology 515

[37] The surface of Ph has a distinct character of smooth 516
 plains and subdued crater morphologies (Figure 14). It has 517
 been suggested that this material may be an eroded volcanic 518
 ash deposit on the basis of its layered, friable surface 519
 character [Hynek *et al.*, 2002, 2003]. Extensive deposits 520
 of eroded friable material have been mapped throughout the 521
 equatorial region, such as within the Medusae Fossae 522
 Formation, and many of these have been proposed to be 523
 ash deposits [Hynek *et al.*, 2003]. In general, however, the 524

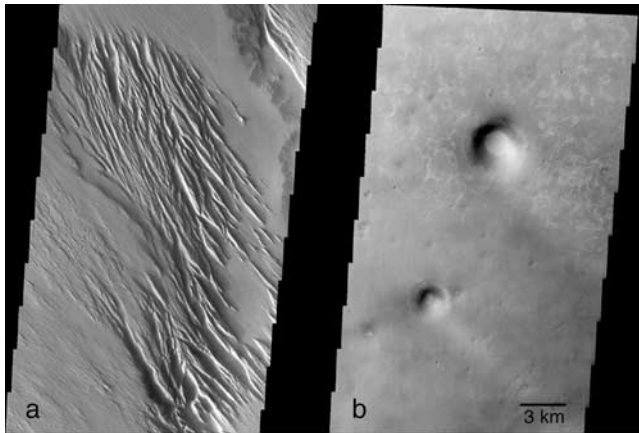


Figure 14. Comparison of the surfaces of proposed ash deposits of (a) the Medusa Fossae unit and (b) the Meridiani hematite-bearing unit Ph. The Meridiani units have a flat surface with unique, subdued crater morphologies and no evidence of yardang-style erosion. The Medusae Fossae materials are characterized by erosion into yardangs. Each image is a portion of a THEMIS visible image with an image resolution of 18 m per pixel. Medusae Fossae image is from V06560001, centered at 5.1°S, 200.3°E; Meridiani image is from V01836001, centered at 1.9°S, 354.3°E.

525 surface of Ph does not appear to erode like putative ash
 526 deposits (Figure 14). *Hynek et al.* [2003] suggest that
 527 the differences may be due to secondary alteration that pro-
 528 duced the observed mineralogy. Alternatively, the Meridiani
 529 unit may not be volcanic ash and was formed by a different
 530 process than the deposition of air fall ash.

531 [38] Unit Ph is also strikingly different from the under-
 532 lying units E and DCT (Figure 12). It erodes in a signifi-
 533 cantly different manner, lacks the connected series of ridges
 534 found in unit E [*Arvidson et al.*, 2003], shows clear
 535 evidence of layering that is unlike units E and DCT, has a
 536 lower thermal inertia, appears to be deposited on both E and
 537 DCT, and contains hematite.

538 [39] Both the Ph and E units were deposited unconformably
 539 on the older cratered terrain [*Hynek et al.*, 2002;
 540 *Arvidson et al.*, 2003]. A series of channels were eroded
 541 into the DCT unit prior to the deposition of Ph [*Newsom et*
 542 *al.*, 2003]. These channels appear to have flowed southward
 543 toward the current location of the Ph unit in mesa M,
 544 suggesting the possible flow of water into a local basin
 545 where this mesa formed.

546 [40] We suggest that while unit Ph lies atop units E and
 547 DCT, its physical and compositional properties point to a
 548 significantly different environment of deposition. *Arvidson*
 549 *et al.* [2003] suggested that Ph and E were deposited
 550 unconformably on top of the older cratered terrains. We
 551 concur with this interpretation, but suggest that Ph was
 552 formed under different conditions and processes than the
 553 underlying E units.

555 3. Discussion

556 [41] The formation modes for the gray crystalline hema-
 557 tite detected by TES were grouped into two classes by

Christensen et al. [2000b, 2001]: (1) chemical precipitation 558
 and (2) thermal oxidation of magnetite-rich volcanic mate- 559
 rials. The chemical precipitation models they proposed were 560
 (1a) low-temperature precipitation of Fe oxides/oxyhydr- 561
 oxides from standing, oxygenated, Fe-rich water, followed 562
 by subsequent alteration to crystalline hematite, (1b) low- 563
 temperature leaching of iron-bearing silicates and other 564
 materials to leave a Fe-rich residue (laterite-style weather- 565
 ing) which is subsequently altered to crystalline hematite, 566
 (1c) precipitation of Fe oxides or crystalline hematite from 567
 Fe-rich circulating fluids of hydrothermal or other origin, 568
 and (1d) formation of crystalline hematitic surface coatings 569
 during weathering. Models 1a and 1b require an alteration 570
 process (e.g., burial metamorphism) to convert Fe oxide/ 571
 hydroxide assemblages (e.g., goethite, red hematite, ferri- 572
 hydrite, and siderite) to crystalline gray hematite. 573

[42] On the basis of the analysis of TES, MOC, and 574
 MOLA data, *Christensen et al.* [2001] could not exclude 575
 any of these models but favored the two models in which 576
 the deposits of crystalline gray hematite were formed either 577
 by chemical precipitation of hematite (or a goethite precu- 578
 sor [*Glotch et al.*, 2004]) from Fe-rich aqueous fluids 579
 under ambient (model 1a) or by hydrothermal processes 580
 (model 1c). Subsequent analysis by *Lane et al.* [2002] 581
 proposed the precipitation of Fe oxides that were metamor- 582
 phosed by burial to platy hematite and subsequently 583
 exposed by erosion. *Hynek et al.* [2002] favored precipita- 584
 tion from Fe-rich circulating fluids (model 1c) or thermal 585
 oxidation of volcanic ash during eruption (model 2). 586
Newsom et al. [2003] suggest, but do not distinguish 587
 between, precipitation from standing water, precipitation 588
 as coatings from groundwater, or oxidation of preexisting 589
 minerals. *Catling and Moore* [2003] favored Fe-rich hydro- 590
 thermal fluids as the emplacement mechanism for the 591
 formation of hematite at Aram Chaos on the basis of both 592
 geochemical and geomorphologic evidence. 593

[43] The close correlation of hematite-bearing material 594
 with specific rock units argues against an external process 595
 of surface coating (model 1d). It is possible that a reaction 596
 occurred between the atmosphere or groundwater and 597
 material in a specific rock unit, but in this case the process 598
 is best characterized by one of the models by which this 599
 material was originally deposited. The lack of any evidence 600
 for extensive surface runoff argues against a surface chemi- 601
 cal leaching process (model 1b). Each of the remaining 602
 three models will be discussed in light of the observations 603
 presented above, with an emphasis on the major points for, 604
 and against, each mechanism. 605

606 3.1. Oxidation of Magnetite-Rich Ash

[44] The oxidation of magnetite-rich ash combines the 607
 hematite precursor (magnetite) and the alteration mecha- 608
 nism (heat of eruption) into a single process. Ash provides 609
 an easily erodible material, and multiple eruption events can 610
 produce the observed variations in layer competency 611
 [*Hynek et al.*, 2002]. However, high-temperature oxidation 612
 of magnetite does not produce spectra that match the TES 613
 observations [*Glotch et al.*, 2004]. In addition, the occur- 614
 rence of hematite in terrestrial volcanic deposits, such as El 615
 Laco, Chile, or Kiirunavaara, Sweden, may be derived from 616
 late-stage hydrothermal activity, rather than in-air oxidation 617
 [*Catling and Moore*, 2003; *Bookstrom*, 1995; *Parak*, 1975]. 618

619 These types of deposits are also dominated by magnetite,
 620 yet this mineral is not detected in the TES observations of
 621 hematite-rich surfaces [Catling and Moore, 2003]. An air
 622 fall deposit can account for the draping of topography, such
 623 as at crater C (Figure 3). The apparent thickness of material
 624 in this crater is comparable to that outside, consistent with
 625 uniform deposition from above. However, the embayment
 626 relationships and the lack of hematite-rich material on the
 627 plains to the south argue against a dispersed air fall deposit.
 628 The truncation of layers in embayment contacts instead
 629 suggests a dense surface flow or subaqueous deposition, and
 630 the lack of material on the plains would require that any
 631 deposited ash has been completely removed. The uniformity
 632 of hematite abundance across the deposit would require a
 633 massive eruption of ash of uniform composition that dif-
 634 ferred from the layer deposited immediately above, and
 635 possibly below (e.g., at R and M), and which differs in
 636 composition and morphology from other possible ash
 637 deposits on Mars. Finally, the coarse-grained basaltic com-
 638 position of the primary component of Ph is not consistent
 639 with a fine-grained, presumably glassy, ash deposit.

640 3.2. Hydrothermal Alteration of Preexisting Rock 641 Units

642 [45] Hydrothermal fluids can dissolve Fe from preexisting
 643 rocks, which can then be precipitated as hematite or as Fe
 644 oxyhydroxides that are subsequently dehydroxylated to
 645 hematite. Both of these mechanisms produce good matches
 646 to the TES spectra [Glotch *et al.*, 2004]. However, the
 647 transition from hematite-rich to hematite-poor material at
 648 the contact between Ph and Pu occurs over a vertical
 649 distance of only several meters. The presence of unaltered
 650 layers immediately above the Ph unit would require that the
 651 proposed alteration did not extend into these layers, despite
 652 occurring over an area more than 150,000 km² in size. This
 653 sharp vertical boundary between a proposed altered unit
 654 (Ph) and one directly above that has little or no hematite
 655 (Pu) is not consistent with a regional hydrothermal process.
 656 It is possible that the hematite-poor unit was deposited after
 657 the alteration occurred. However, there is no evidence for
 658 this in an unconformity or significant change in unit
 659 characteristics between Ph and Pu. Finally, the lack of a
 660 systematic lateral variation in hematite abundance across Ph
 661 suggests that there was no significant variation in the degree
 662 of alteration across this large area and that there was no
 663 apparent center or focus of this alteration, again inconsistent
 664 with regional alteration.

665 [46] If hydrothermal alteration did occur, then several
 666 sources of the altering fluids can be considered. The fluids
 667 could have originated from a regional source below Ph, but
 668 the presence of unaltered basaltic material below Ph (unit E)
 669 makes this source unlikely. The fluids could have moved
 670 laterally through Ph, confined at the base by an imperme-
 671 able layer that could have been the high-inertia subunit of
 672 Ph or the Etched unit. However, a significant difficulty with
 673 this model is the presence of hematite within distant,
 674 preexisting craters in different terrains and at significantly
 675 different elevations. It is unlikely that a single impermeable
 676 layer would exist both inside and outside the craters, that
 677 fluids would migrate through the disrupted crater walls, or
 678 that fluids would migrate through Ph only in these different
 679 locales. The fluids could have come from above, such as

680 from the melting of an overlying snow or ice deposit. These
 681 waters would melt and move downward, be heated by some
 682 thermal source, dissolve iron, and then precipitate hematite
 683 or its precursor. However, with this model it is again
 684 difficult to account for the sharp transition from hematite-
 685 poor to hematite-rich materials within several meters of
 686 elevation as seen at R and M.

687 3.3. Deposition of Hematite or Precursor Fe Oxides or 688 Oxyhydroxides in Water

689 [47] The deposition of hematite or precursor Fe oxide/
 690 hydroxides in water can resolve many of the difficulties
 691 discussed above. The formation of goethite, followed by
 692 dehydroxylation to hematite, provides the best match to the
 693 observed TES spectra [Glotch *et al.*, 2004]. Deposition from
 694 standing water could account for the hematite occurring in a
 695 thin, widespread, uniform, friable unit, with deposition of
 696 hematite, or precursor Fe oxide/hydroxides [Glotch *et al.*,
 697 2003], occurring as the temperature, Ph, or Eh of the water
 698 changed with time. In this mechanism the sharp boundaries
 699 at the top, and possibly bottom, of the hematite layer were
 700 produced by changes in depositional environment, rather
 701 than requiring changes in hydrothermal alteration over
 702 meter-scale vertical distances. Deposition of a precursor
 703 material in standing water would account for the large
 704 lateral, but small vertical, extent of the hematite layer. The
 705 currently exposed surface of Meridiani varies in elevation
 706 by ~100 m and in hematite abundance from ~5 to 20%.
 707 The variations may reflect local erosion, with hematite
 708 varying in abundance as it is removed or slightly concen-
 709 trated as a surface lag as the hematite-bearing layer is
 710 deflated. The similarity in the character of the hematite-
 711 bearing unit in Ph with Pu could be explained by their being
 712 deposited under similar environments that differed only in
 713 the precipitation of relatively minor amounts of Fe oxides.
 714 Deposition of Fe oxide precursor was proposed by Lane *et*
 715 *al.* [2002], followed by burial metamorphism and erosion to
 716 expose the material. Recent laboratory measurements indi-
 717 cate that burial metamorphism is not required to reproduce
 718 the hematite spectral character observed by TES [Glotch *et*
 719 *al.*, 2004].

720 [48] Burns [1993] initially suggested that banded iron
 721 formation (BIF) may have occurred on Mars on the basis of
 722 the likely occurrence of iron-rich fluids. This possibility has
 723 been explored for a range of chemical, photostimulated, and
 724 biologic oxidation to produce precursor Fe oxides, followed
 725 by low-grade thermal transition to hematite (see review by
 726 Catling and Moore [2003]). On the Earth, precipitation of
 727 Fe oxyhydroxides from iron-rich water followed by low-
 728 temperature, low-pressure dehydroxylation has been pro-
 729 posed for the formation of hematite in banded iron
 730 formations [Krapez *et al.*, 2003]. In a model developed
 731 for the Hamersley Province of Australia the precursor sedi-
 732 ments to BIF are interpreted to have been hydrothermal
 733 muds composed of iron-rich oxyhydroxides, smectite, and
 734 siderite that were deposited on the flanks of submarine
 735 volcanoes and transported by density currents [Krapez *et*
 736 *al.*, 2003]. Hematite spheroids in these sediments closely
 737 resemble those found in modern Red Sea iron oxide
 738 deposits [Butuzova *et al.*, 1990] and are likely diagenetic
 739 transformations of iron oxyhydroxide muds [Krapez *et al.*,
 740 2003; Bischoff, 1969a, 1969b]. Alternating Fe oxide and

741 silica layers in the Hamersley BIF are compacted density
742 current laminations, with the chert being diagenetic and
743 developed during burial [Krapez *et al.*, 2003]. The con-
744 ditions on Mars may have been sufficiently different from
745 the terrestrial examples for silica not to have been precip-
746 itated, resulting in a sequence consisting only of Fe oxides
747 [e.g., Fernández-Remolar *et al.*, 2004].

748 [49] An aqueous origin for the hematite deposits in
749 Meridiani has been proposed on the basis of analogy to
750 the Rio Tinto iron formations of Spain [Fernández-Remolar
751 *et al.*, 2004]. This extreme acidic environment has water
752 that is rich in ferric iron and sulfate that produces sediments
753 dominated by ferric oxyhydroxides and sulfate minerals,
754 with no silica phases [Fernández-Remolar *et al.*, 2004].
755 These iron formations suggest that the iron phase has
756 changed over time from iron oxyhydroxides and sulfates
757 to hematite-goethite-dominated associations through dehy-
758 droxylation and desulfation [Fernández-Remolar *et al.*,
759 2004]. This mechanism would account for the lack of other
760 minerals detected by the TES in Meridiani and accounts for
761 the development of coarse-grained crystalline hematite
762 [Fernández-Remolar *et al.*, 2004]. This model accounts
763 for the lack of silica in Meridiani by the occurrence of a
764 standing body of water fed by underground iron-rich sources
765 whose chemistry and thermodynamics favored precipitation
766 of iron-bearing phases but not silica [Fernández-Remolar
767 *et al.*, 2004].

768 [50] To form hematite from standing water on Mars, both
769 a source of oxidation and the necessary conditions for
770 dehydroxylation to hematite are required [Catling and
771 Moore, 2003]. Fine-grained goethite is thermodynamically
772 unstable relative to hematite plus water [Berner, 1969;
773 Langmuir, 1971]. Laboratory studies have shown that
774 dehydroxylation to hematite can occur within a few weeks
775 in water at temperatures between 70° and 130°C [Tunell and
776 Posnjak, 1931; Catling and Moore, 2003; Johnston and
777 Lewis, 1983; Vorobyeva and Melnik, 1977; Schmalz, 1959;
778 Wefers, 1966]. Thermodynamic data of Diakonov *et al.* were
779 used by Catling and Moore [2003] to construct a phase
780 diagram for goethite-hematite in which the transition to
781 hematite occurs at 100°C. Thermodynamic calculations by
782 Berner [1969], however, indicate that the maximum tem-
783 perature at which fine-grained goethite is stable relative to
784 hematite is ~40°C. Natural occurrences where the temper-
785 atures are constrained by oxygen isotope evidence suggest
786 that the temperatures of these natural systems are >100°C
787 [Catling and Moore, 2003]. However, the transformation
788 from iron oxyhydroxide phases to dehydroxylated hematite
789 in the Rio Tinto, Spain, system has been suggested by
790 Fernández-Remolar *et al.* [2004] to imply that hematite may
791 be formed by dehydration pathways in shallow diagenesis
792 and lower-temperature conditions rather than deep burial. In
793 summary, the available thermodynamic, laboratory, and
794 field data suggest that the transition from goethite to
795 hematite in saturated conditions can occur at temperatures
796 between 40° and 100°C. These temperatures imply modest
797 heating and relatively low-temperature diagenesis. The
798 source of this heat may have been burial to depths of
799 several kilometers [Catling and Moore, 2003] or may have
800 been produced by subsurface magmatic heat. Evidence for
801 significant subsurface heating in Meridiani Planum is seen
802 in the basaltic volcanic plains that comprise the units below

Ph [Christensen *et al.*, 2000b; Hynes *et al.*, 2002; Arvidson 803
et al., 2003] and the melting of vast amounts of subsurface 804
ice in equatorial chaotic terrains and catastrophic outflow 805
channels. 806

[51] An obvious argument against precipitation from a
807 standing body of water is the present lack of a confining 808
topographic rise on the northern margin of Ph. Hynes *et al.* 809
[2002] and Arvidson *et al.* [2003] have suggested that Ph is 810
part of thick set of units (P1–P3, Etched) extending over 811
hundreds of kilometers to the north that were deposited on a 812
regional slope and have since been extensively eroded. 813
Phillips *et al.* [2001] argued that this slope formed during 814
the Noachian prior to the deposition of Ph on the basis of the 815
presence of preexisting channels that preferentially flowed 816
down this regional slope. Crater counts have confirmed that 817
the hematite unit is Noachian in age [Hynes and Phillips, 818
2001; Hynes *et al.*, 2002; Lane *et al.*, 2003] and formed near 819
the time that this slope was developing. If all of the units in 820
Meridiani were deposited in water, then the basin boundary 821
would also have to be 500–600 km to the north, where the 822
current topography is ~600 m below the hematite layer 823
[Hynes *et al.*, 2002]. However, the hematite-bearing unit 824
differs significantly from the etched unit E in morphology, 825
thermal inertia, erosional style, heterogeneity, and hematite 826
abundance, suggesting that these two units were deposited 827
in significantly different environments. 828

[52] An alternative scenario is suggested here, in which 829
unit Ph, but not unit E, was deposited within a series of 830
local, water-filled basins. Arvidson *et al.* [2003] interpreted 831
the Etched unit to be lava flows subjected to extension that 832
fractured the flows into polygons, followed by emplacement 833
of dikes and flows and further extension to form horst- 834
graben patterns. They interpret units P and Ph to be a 835
subsequent stage of the volcanoclastic activity that blanketed 836
the Etched unit. The model proposed here suggests a similar 837
set of events, except that Ph was deposited in water, rather 838
than as a volcanoclastic layer. In both models the materials 839
that make up the Etched and Ph units are significantly 840
different. We argue that the deposition of Ph in water or as 841
volcanoclastic material cannot be distinguished on the basis 842
of stratigraphy. What is important to the standing water 843
model is that units Ph and Etched were deposited in 844
different environments. The apparent deposition of Ph 845
directly on unit DCT (Figure 10) indicates that Ph was 846
deposited in regions where unit E was not, providing 847
additional evidence that Ph was deposited in a different 848
manner than unit E. We propose that units Ph and E were 849
deposited under different conditions and that only the 850
relatively thin Ph unit, not the entire sequence of Etched 851
units, was deposited in water. In this case, only a basin of 852
the size necessary to contain the Ph unit needs to be 853
considered. 854

[53] In the standing water model proposed here the 855
coarse-grained basalt that makes up the majority of the 856
material of Ph was deposited as clastic sediments within 857
these bodies of water. The northern margin of Ph from ~1°S 858
at 356°E and 1°N at 359°E (Figure 3) represents the 859
northernmost extent of the main basin. This local basin 860
may be related to the large impact basin inferred from 861
MOLA data [Frey, 2003; Newsom *et al.*, 2003]. Outliers 862
of hematite-rich material to the north, west, and south are 863
proposed to have been deposited within craters that formed 864

865 separate closed basins. The deposition of hematite within
866 these separate bodies of water accounts for the lack of
867 hematite observed on the intracrater plains.

868 [54] Morphologic evidence from MOC and THEMIS
869 imaging has suggested the occurrence of flow and deposi-
870 tion into standing water in closed basins elsewhere on Mars
871 [Malin and Edgett, 2003; Moore et al., 2003]. In many
872 locations, Ph lies within a local trough (Figures 13a and 13b),
873 and in places where Ph is higher than its surroundings, this
874 elevation difference is less than 50–100 m (Figures 13a and
875 13b). If Ph was deposited contemporaneously with regional
876 tilting, then minor tilting of the region, i.e., several hundred
877 meters over several hundred kilometers, could have oc-
878 curred after the hematite units were deposited. More impor-
879 tantly, the large amount of erosion that has occurred in this
880 region makes it unlikely that the remains of the original
881 bounding topography of a closed basin would be preserved
882 today. An excellent example of the large-scale erosion that
883 has occurred in this region can be seen by the presence of
884 several large, circular occurrences of Ph standing as
885 elevated mesas (Figure 5). These units were likely deposited
886 within large (tens of kilometer diameter) craters, and the
887 crater walls that originally bounded them have been com-
888 pletely eroded away (e.g., Figure 5), producing an inverted
889 topography of highstanding circular mesas.

891 4. Summary and Predictions for the MER Rovers

892 [55] In summary, the three leading candidates for the
893 formation of the hematite-bearing unit in Meridiani Planum
894 all have shortcomings to varying degrees. The model of
895 oxidation of volcanic ash suffers from the poor spectral fit
896 to a magnetite precursor, the dissimilarities of the hematite
897 unit to proposed ash deposits elsewhere, and the spectral
898 dissimilarity between volcanic ash and basaltic sediments.
899 The hydrothermal alteration model suffers primarily from
900 the need to reconcile the very confined vertical extent of the
901 hematite layer over huge distances and across disconnected
902 occurrences. A model of the deposition of precursor Fe
903 oxyhydroxides in water-filled basins requires minor erosion
904 or tilting in order to account for the present-day lack of a
905 completely closed basin for the main Ph unit. We favor this
906 model of deposition in standing water, however, because it
907 does account for the following observations: (1) the occur-
908 rence of a thin hematite unit over an area $\sim 150,000$ km²
909 in size with sharp upper (and possibly lower) contacts; (2)
910 spectral evidence for goethite as a precursor to hematite; (3)
911 the presence of a finely layered, friable texture on Ph in
912 distinct contrast to the morphology of the Etched units on
913 which it lies; (4) embayment relationships on the southern
914 margin of Ph; (5) the occurrence of remnants of hematite-
915 bearing units within isolated craters surrounding of the main
916 Ph unit, and the lack of these units on the intracrater plains;
917 (6) the lack of other hydrothermal minerals; (7) the presence
918 of low-albedo, coarse-grained basalt, rather than ash, as the
919 major component of the hematite-bearing unit; and (8) the
920 differences in morphology between Ph and proposed ash
921 units.

922 [56] Crystalline hematite is currently exposed only in
923 Meridiani, Aram Chaos, and a few locations within Valles
924 Marineris [Christensen et al., 2001]. Thus the formation
925 of hematite-bearing material appears to have required a

specific set of conditions that may have occurred only 926
rarely through Mars history. The occurrence of unweathered 927
olivine, pyroxene, and feldspar in basalts throughout the 928
equatorial region provides strong evidence that extensive 929
aqueous weathering has not occurred on Mars [Christensen 930
et al., 2000a, 2003a; Hoefen et al., 2003]. Thus the presence 931
of a small number of bodies of standing water appears to 932
represent brief, localized phenomena set against the back- 933
drop of a cold, frozen planet. 934

[57] It is expected that in situ observations from the MER 935
Opportunity rover will address some of these questions. 936
The origin of hematite from oxidation of ash would be 937
supported by observations from microscopic and panoramic 938
imaging of the rock and sediment textures indicative of ash 939
and by the detection of precursor magnetite or partially 940
hematitized magnetite grains using infrared and Mössbauer 941
spectroscopy [Squyres et al., 2003]. A hydrothermal origin 942
can be tested using the Miniature Thermal Emission Spec- 943
trometer [Christensen et al., 2003b] and Mössbauer spec- 944
trometer to look for other associated hydrothermal 945
minerals, and microscopic images can be used to determine 946
if the hematite occurs along grain boundaries and in 947
veinlets indicative of postdepositional fluid migration and 948
alteration. The origin of hematite in water-filled basins can 949
be tested by looking for large- and small-scale sedimentary 950
structures. Mineralogic, elemental, or textural evidence can 951
be used to detect a precipitated hematite precursor, such as 952
goethite, that was deposited as a continuous layer, rather 953
than from a later hydrothermal fluid. Rounded grains or 954
hematite/Fe oxyhydroxide spheroids would be compelling 955
evidence for this model. In addition, the occurrence of 956
coarse-grained basalt as a major component and as a 957
sedimentary, rather than a primary, igneous component 958
can be used to distinguish a sedimentary versus volcanic 959
origin. 960

[58] **Acknowledgments.** We wish to thank the engineers at Raytheon 961
Santa Barbara Remote Sensing for the development of a superb THEMIS 962
instrument, the engineers at Lockheed Martin Astronautics for the devel- 963
opment and operation of an excellent Odyssey spacecraft, and the engineers 964
and scientists at the Jet Propulsion Laboratory for the operation of the 965
highly successful Odyssey mission. We thank the ISIS Software Develop- 966
ment Team at the U.S.G.S. in Flagstaff, AZ, led by Jim Torson for the 967
development of the ISIS geometry software, and the THEMIS mission 968
operations and software development groups at Arizona State University, 969
led by Greg Mehall, Noel Gorelick, Kelly Bender, Loral Cherednik, 970
Andras Dombovari, and Kim Murray for the excellent operation of the 971
THEMIS investigation. Noel Gorelick, Michael Weiss-Malik, and Ben 972
Steinberg led the development of the JMARS data analysis software used 973
extensively in this study. Noel Gorelick produced the mosaics used in 974
Figures 1 and 2. We thank Tim Glotch, Dick Morris, Trevor Graff, and 975
Mike Wyatt for helpful discussions. Detailed reviews by Brian Hynek and 976
Jeffery Moore significantly improved this manuscript. This work was 977
supported by the 2001 Mars Odyssey Science Office and the Mars Global 978
Surveyor Science Office. 979

980 References

- Arvidson, R. E., F. P. Seelos IV, K. S. Deal, N. O. Snider, J. M. Kieniewicz, 981
B. M. Hynek, M. T. Mellon, and J. B. Garvin (2003), Mantled and 982
exhumed terrains in Terra Meridiani, Mars, *J. Geophys. Res.*, 108(E12), 983
8073, doi:10.1029/2002JE001982. 984
Bandfield, J. L. (2002), Global mineral distributions on Mars, *J. Geophys.* 985
Res., 107(E6), 5042, doi:10.1029/2001JE001510. 986
Bandfield, J. L., V. E. Hamilton, and P. R. Christensen (2000), A global 987
view of Martian volcanic compositions, *Science*, 287, 1626–1630. 988
Berner, R. A. (1969), Goethite stability and the origin of red beds, *Cosmo-* 989
chim. Acta., 33, 267–273. 990
Bischoff, J. L. (1969a), Goethite-hematite stability relations with relevance 991
to sea water and the Red Sea brine system, in *Hot Brines and Recent* 992

- 993 *Heavy Metal Deposits in the Red Sea*, edited by E. T. Degens and D. A.
 994 Ross, pp. 402–406, Springer-Verlag, New York.
- 995 Bischoff, J. L. (1969b), Red Sea geothermal brine deposits: Their mineral-
 996 ology, chemistry, and genesis, in *Hot Brines and Recent Heavy Metal*
 997 *Deposits in the Red Sea*, edited by E. T. Degens and D. A. Ross,
 998 pp. 368–401, Springer-Verlag, New York.
- 999 Bookstrom, A. A. (1995), Magmatic features of iron-ores of the Kiruna type
 1000 in Chile and Sweden—Ore textures and magnetite geochemistry—A
 1001 discussion, *Econ. Geol.*, **90**, 469–473.
- 1002 Burns, R. G. (1993), Rates and mechanisms of chemical weathering of
 1003 ferromagnesian silicate minerals on Mars, *Geochim. Cosmochim. Acta*,
 1004 **57**, 4555–4574.
- 1005 Butuzova, G. Y., V. A. Drits, A. A. Morozov, and A. I. Gorschov, (1990),
 1006 Processes of formation of iron-manganese oxyhydroxides in the Atlantic-
 1007 II and Thetis Deepes of the Red Sea, in *Sediment-Hosted Mineral Depos-*
 1008 *its*, edited by J. Parnell, Y. Lianjun, and C. Changming, *Spec. Publ. Int.*
 1009 *Assoc. Sedimentol.*, **11**, 57–72.
- 1010 Catling, D. C., and J. M. Moore (2003), The nature of coarse-grained
 1011 crystalline hematite and its implications for the early environment of
 1012 Mars, *Icarus*, **165**, 277–300.
- 1013 Christensen, P. R., J. L. Bandfield, M. D. Smith, V. E. Hamilton, and R. N.
 1014 Clark (2000a), Identification of a basaltic component on the Martian
 1015 surface from Thermal Emission Spectrometer data, *J. Geophys. Res.*,
 1016 **105**, 9609–9622.
- 1017 Christensen, P. R., et al. (2000b), Detection of crystalline hematite mineral-
 1018 ization on Mars by the Thermal Emission Spectrometer: Evidence for
 1019 near-surface water, *J. Geophys. Res.*, **105**, 9623–9642.
- 1020 Christensen, P. R., M. C. Malin, R. V. Morris, J. L. Bandfield, and M. D.
 1021 Lane (2001), Martian hematite mineral deposits: Remnants of water-
 1022 driven processes on early Mars, *J. Geophys. Res.*, **106**, 23,873–23,885.
- 1023 Christensen, P. R., et al. (2003a), Morphology and composition of the sur-
 1024 face of Mars: Mars Odyssey THEMIS results, *Science*, **300**, 2056–2061.
- 1025 Christensen, P. R., et al. (2003b), Miniature Thermal Emission Spectro-
 1026 meter for the Mars Exploration Rovers, *J. Geophys. Res.*, **108**(E12),
 1027 8064, doi:10.1029/2003JE002117.
- 1028 Edgett, K. S., and T. J. Parker (1997), Water on early Mars: Possible sub-
 1029 aqueous sedimentary deposits covering ancient cratered terrain in western
 1030 Arabia and Sinus Meridiani, *Geophys. Res. Lett.*, **24**, 2897–2900.
- 1031 Fergason, R. L., and P. R. Christensen (2003), Thermal inertia using
 1032 THEMIS infrared data, *Lunar Planet. Sci.*, **XXXIV**, abstract 1785.
- 1033 Fernández-Remolar, J. Gómez-Elvira, F. Gómez, E. Sebastian, J. Martín,
 1034 J. A. Manfredi, J. Torres, C. G. Kessler, and R. Amils (2004), The Tinto
 1035 River, an extreme acidic environment under control of iron, as an analog
 1036 of the Terra Meridiani hematite site of Mars, *Planet. Space Sci.*, **52**, 239–
 1037 248.
- 1038 Frey, H. V. (2003), Buried impact basins and the earliest history of Mars,
 1039 in *Sixth International Conference on Mars* [CD-ROM], abstract 1979,
 1040 Lunar and Planet. Inst., Houston, Tex.
- 1041 Glotch, T. D., R. V. Morris, T. G. Sharp, and P. R. Christensen (2003),
 1042 Characterization of the effects of precursor mineralogy on hematite spec-
 1043 tra: Application to Martian hematite mineralization, *Lunar Planet. Sci.*,
 1044 **XXXIV**, abstract 2008.
- 1045 Glotch, T. D., R. V. Morris, P. R. Christensen, and T. G. Sharp (2004),
 1046 Effect of precursor mineralogy on the thermal infrared emission spectra
 1047 of hematite: Application to Martian hematite mineralization, *J. Geophys.*
 1048 *Res.*, **109**, doi:10.1029/2003JE002224, in press.
- 1049 Hoefen, T., R. N. Clark, J. L. Bandfield, M. D. Smith, J. C. Pearl, and P. R.
 1050 Christensen (2003), Discovery of olivine in the Nili Fossae region of
 1051 Mars, *Science*, **302**, 627–630.
- 1052 Hynek, B. M., and R. J. Phillips (2001), Evidence for extensive denudation
 1053 of the Martian highlands, *Geology*, **29**, 407–410.
- 1054 Hynek, B. M., R. E. Arvidson, and R. J. Phillips (2002), Geologic setting
 1055 and origin of Terra Meridiani hematite deposit on Mars, *J. Geophys. Res.*,
 1056 **107**(E10), 5088, doi:10.1029/2002JE001891.
- 1057 Hynek, B. M., R. J. Phillips, and R. E. Arvidson (2003), Explosive volcan-
 1058 ism in the Tharsis region: Global evidence in the Martian geologic record,
 1059 *J. Geophys. Res.*, **108**(E9), 5111, doi:10.1029/2003JE002062.
- 1060 Johnston, J. H., and D. G. Lewis (1983), A detailed study of the transition
 1061 of ferrihydrite to hematite in an aqueous solution at 92°C, *Geochim.*
 1062 *Cosmochim. Acta*, **47**, 1823–1831.
- Krapez, B., M. E. Barley, and A. L. Pickard (2003), Hydrothermal and
 1063 resedimented origins of the precursor sediments to banded iron
 1064 formation: Sedimentological evidence from the Early Paleoproterozoic
 1065 Brockman Supersquence of Western Australia, *Sedimentology*, **50**,
 1066 979–1011, doi:10.1046/j.1365-3091.2003.0594.
 1067
- Lane, M. D., R. V. Morris, S. A. Mertzman, and P. R. Christensen (2002),
 1068 Evidence for platy hematite grains in Sinus Meridiani, Mars, *J. Geophys.*
 1069 *Res.*, **107**(E12), 5126, doi:10.1029/2001JE001832.
 1070
- Lane, M. D., P. R. Christensen, and W. K. Hartmann (2003), Utilization of
 1071 the THEMIS visible and infrared imaging data for crater population
 1072 studies of the Meridiani Planum landing site, *Geophys. Res. Lett.*,
 1073 **30**(14), 1770, doi:10.1029/2003GL017183.
 1074
- Langmuir, D. (1971), Particle size effect on the reaction goethite = hematite
 1075 + water, *Am. J. Sci.*, **271**, 147–156.
 1076
- Malin, M. C., and K. S. Edgett (2003), Evidence for persistent flow and
 1077 aqueous sedimentation on early Mars, *Science*, **302**, 1931–1934.
 1078
- Mellon, M. T., B. M. Jakosky, H. H. Kieffer, and P. R. Christensen (2000),
 1079 High resolution thermal inertia mapping from the Mars Global Surveyor
 1080 Thermal Emission Spectrometer, *Icarus*, **148**, 437–455.
 1081
- Melosh, H. J. (1989), *Impact Cratering, A Geologic Process*, 78 pp., Ox-
 1082 ford Univ. Press, New York.
 1083
- Moore, J. M., A. D. Howard, W. E. Dietrich, and P. M. Schenk (2003),
 1084 Martian Layered Fluvial Deposits: Implications for Noachian Climate Scen-
 1085 arios, *Geophys. Res. Lett.*, **30**(24), 2292, doi:10.1029/2003GL019002.
 1086
- Morris, R. V., M. D. Lane, S. Mertzman, T. D. Shelfer, and P. R. Christensen
 1087 (2000), Chemical and mineralogical purity of Sinus Meridiani hematite,
 1088 *Lunar Planet. Sci.* [CD-ROM], **XXXI**, abstract 1618.
 1089
- Newsom, H. E., C. A. Barber, T. M. Hare, R. T. Schelble, V. A. Sutherland,
 1090 and W. C. Feldman (2003), Paleolakes and impact basins in southern
 1091 Arabia Terra, including Meridiani Planum: Implications for the formation
 1092 of hematite deposits on Mars, *J. Geophys. Res.*, **108**(E12), 8075,
 1093 doi:10.1029/2002JE001993.
 1094
- Parak, T. (1975), Kiruna type ores are “intrusive-magmatic ores of the
 1095 Kiruna type”, *Econ. Geol.*, **70**, 1242–1248.
 1096
- Phillips, R. J., et al. (2001), Ancient geodynamics and global-scale hydrology
 1097 of Mars, *Science*, **291**, 2587–2591.
 1098
- Presley, M. A., and R. E. Arvidson (1988), Nature and origin of materials
 1099 exposed in the Oxia Palus-Western Arabia-Sinus Meridiani region, Mars,
 1100 *Icarus*, **75**, 499–517.
 1101
- Presley, M. A., and P. R. Christensen (1997), Thermal conductivity
 1102 measurements of particulate materials, Part II: Results, *J. Geophys.*
 1103 *Res.*, **102**, 6566–6651.
 1104
- Ramsey, M. S., and P. R. Christensen (1998), Mineral abundance determi-
 1105 nation: Quantitative deconvolution of thermal emission spectra, *J. Geop-*
 1106 *hys. Res.*, **103**, 577–596.
 1107
- Ruff, S. W., and P. R. Christensen (2002), Bright and dark regions on
 1108 Mars: Particle size and mineralogical characteristics based on Thermal
 1109 Emission Spectrometer data, *J. Geophys. Res.*, **107**(E12), 5127,
 1110 doi:10.1029/2001JE001580.
 1111
- Schmalz, R. A. (1959), A note on the system Fe₂O₃-H₂O, *J. Geophys. Res.*,
 1112 **64**, 575–579.
 1113
- Smith, D. E., et al. (2001), Mars Orbiter Laser Altimeter: Experiment
 1114 summary after the first year of global mapping of Mars, *J. Geophys.*
 1115 *Res.*, **106**, 23,689–23,722.
 1116
- Squyres, S. W., et al. (2003), Athena Mars rover science investigation,
 1117 *J. Geophys. Res.*, **108**(E12), 8062, doi:10.1029/2003JE002121.
 1118
- Tunell, G., and E. Posnjak (1931), The stability relations of goethite and
 1119 hematite, *Econ. Geol. Bull. Soc. Econ. Geol.*, **26**(3), 337–343.
 1120
- Vorobyeva, K. A., and Y. P. Melnik (1977), An experimental study of the
 1121 system of Fe₂O₃-H₂O at T = 100–200°C and P up to 9 kilobars, *Geo-*
 1122 *chem. Int.*, **8**, 108–115.
 1123
- Wefers, K. (1966), On the system Fe₂O₃-H₂O. Part 1, *Deutsch. Keram.*
 1124 *Ges.*, **43**, 677–702.
 1125

P. R. Christensen and S. W. Ruff, Department of Geological Sciences, 1126
 Campus Box 6305, Arizona State University, Tempe, AZ 85287-6305, 1128
 USA. (phil.christensen@asu.edu) 1129